Metal-Organic Framework on Fullerene (MOFOF) as a Hierarchical Composite by the Integration of Coordination Chemistry and Supramolecular Chemistry

Biswa Nath Bhadra,[†] *Lok Kumar Shrestha,* [†,¶,*] *Renzhi Ma,* [†] *Jonathan P. Hill,* [†] *Yusuke Yamauchi,*[⊥,±,Ω] *and Katsuhiko Ariga*[†,‡,*]

[†]Research Center for Materials Nanoarchitectonics (WPI-MANA), National Institute for Materials Science (NIMS), 1-1 Namiki, Tsukuba, Ibaraki 305-0044, Japan

[¶]Department of Materials Science, Institute of Pure and Applied Sciences, University of Tsukuba, 1-1-1, Tennodai, Tsukuba 305-8573, Ibaraki, Japan

[⊥]Department of Materials Process Engineering, Graduate School of Engineering, Nagoya University, Nagoya 464−8603, Japan

[±]Department of Chemical and Biomolecular Engineering, Yonsei University, 50 Yonsei-ro, Seodaemun-gu, Seoul 03722, South Korea

[Ω]0Australian Institute for Bioengineering and Nanotechnology (AIBN) and School of Chemical Engineering, The University of Queensland, Brisbane, Queensland 4072, Australia

[‡]Department of Advanced Materials Science, Graduate School of Frontier Sciences, The University of Tokyo, 5-1-5 Kashiwanoha, Kashiwa, Chiba 277-8561, Japan

*Corresponding authors:
Lok Kumar Shrestha (Email: SHRESTHA.Lokkumar@nims.go.jp)
Katsuhiko Ariga (Email: ARIGA.Katsuhiko@nims.go.jp)

ABSTRACT. There is a synergy between coordination chemistry and supramolecular chemistry that has led to the development of innovative hierarchical composites with diverse functionalities. Here, we present a novel approach for the synthesis and characterization of Metal-Organic Framework on Fullerene (MOFOF) composites, achieved through the integration of coordination chemistry and supramolecular chemistry principles. The hierarchical nature of MOFOF harnesses the inherent properties of metal-organic frameworks and fullerenes. The two-step synthesis procedure involves controlled assembly of fullerenes as tube-like nanostructures (fullerene nanotube: FNT), their surface functionalization, and on-surface growth of MOF (in this case, ZIF-67). The method permits precise tuning of morphology, effective distribution of MOF-on-FNT, and tight compositional control. The materials were comprehensively structurally characterized using electron microscopy, spectroscopic techniques, and other methods to elucidate the unique features and interactions within the MOFOF composites. The main findings reveal that the novel synthesis and characterization of MOFOF composites demonstrate the successful integration of coordination chemistry and supramolecular chemistry for the designing and fabricating advanced hierarchical composites with tailored properties, including micro- and mesopores channels, interfacial facets, and defect sites. These properties are expected to lead to numerous potential applications, such as gas storage and separation, catalysis, sensing, energy storage, and environmental remediation. However, only the capability of acid vapor sensing was tested and described here.

KEYWORDS. hierarchical composite, metal-organic framework on fullerene, well-distribution, coordination chemistry, supramolecular chemistry

INTRODUCTION

Metal-organic frameworks (MOFs) have emerged as a class of crystalline porous materials composed of metal ions or clusters connected by organic ligands.[1,2] They offer remarkable properties based on a network of interconnected pores and channels that establish large surface area, tunable porosity, and exceptional structural diversity. These attributes render MOFs promising candidates for various applications, including adsorption,[3,4] gas storage,[5] separation,[6] and sensing.[7] However, MOFs often encounter limitations such as low stability, poor selectivity, diffusion constraints, lack of active sites, and limited conductivity. By incorporating MOFs into composites with other substances, these properties can be enhanced, leading to improved functionalities and new applications. These properties can be further enhanced, leading to improved functionalities and new applications over the MOFs.[8–12] To date, several types of MOF composites, including polymer-MOFs,[13,14] nanoparticle-MOFs,[15] MOF-membranes,[16] and MOF-carbon composites,[17] are available. These MOF composites have gained significant attention due to their tunable properties and versatile applications.[14–22] However, challenges and limitations remain in fabricating MOF composites that exhibit strong interactions with additional components, high stability, uniform coatings, maintaining structural integrity, and well-controlled morphology. Ongoing research addressing these challenges and limitations to create novel composites with enhanced functionalities focuses on exploringcombinations of MOFs with other materials.

Nanoarchitectonics involves the controlled assembly of nanoscale building blocks to create functional materials with tailored properties.[23–25] Fullerene nanoarchitectonics refers to the design, synthesis, and manipulation of nanostructures based on fullerene molecules.[26,27] Fullerene is a unique carbon allotrope with a hollow spherical structure that exhibits intriguing electronic properties and chemical reactivity, making it an intriguing component for composite materials. As

a consequence, the combination of fullerene nanoarchitectonics with MOFs could lead to the development of advanced composites with unique properties and functionalities by the integration of coordination chemistry and supramolecular chemistry. Pristine fullerenes such as C_{60} and C_{70} can be obtained in various nanocrystalline morphologies by using interfacial self-assembly based on the varying solubilities of fullerenes in different solvents. Although this methodology, also referred to as liquid-liquid interfacial precipitation (LLIP), is simple, modification of solvent combinations or precipitation conditions can be used to prepare fullerenes in a wide range of crystal forms including spheres,[28] rods,[29] whiskers,[30] tubes,[31] cubes,[32,33] two-dimensional sheets,[34] amongst others.[35,36] Synthetically modified fullerenes can also be assembled into more exotic forms such as cell-like spherical vesicular structures,[37] and exhibit shape-shifting behavior.[38] In contrast to MOF-composites based on carbon nanomaterials such as carbon nanotubes (CNT) or graphene oxide (GO) which have specific morphologies,[39–41] the chemical surface modification of fullerene nanostructures and their incorporation into MOF-composites has not been investigated despite its large potential for the development of shape-controlled materials having tailored compositions.

To date, the MOF-fullerene composites have generally been prepared by encapsulation and confinement of fullerene guests at the interiors of MOF pores.[42–47] However, the alternative approach of embedding MOFs into surface-modified fullerene nanostructures has yet to be achieved. MOF composites with carbon nanomaterials (e.g., CNT, GO, and rGO.) often lack morphological integrity, suffer from uneven dispersion, and fail to maintain robust attachment. Therefore, preparing MOF-on-fullerene (MOFOF) composites will not only establish a new class of morphology controlled composite materials but will also offer nanoarchitecture-controlled

composites with prospects in a range of advanced technological applications including gas storage and separation, catalysis, sensing, energy storage, and environmental applications.

In this paper, we focus on the synthesis, and characterization of MOFOF composites by the strategic integration of coordination chemistry and supramolecular chemistry principles. By judiciously combining these two fields, we aim to harness the complementary attributes of MOFs and fullerenes, thereby enabling precise control over the hierarchical structure and functional properties of the resulting composites. Typically, ZIF-67 and fullerene nanotubes (FNT) were chosen as representative MOF and fullerene nanostructure, respectively, to design and synthesize the MOFOF composite. ZIF-67 was selected because it can be easily synthesized at room temperature and features abundant active sites, unsaturated metal coordination sites, and micropores. Meanwhile, FNT is sufficiently large to accommodate nanosized ZIF-67 on its surface and within its cavities. A two-step method was developed to synthesize the MOFOF composites with varying compositions or different FNT and ZIF-67 ratios, e.g., Co^{2+}/C_{60} ratios of 0.5, 1.0, 1.5, and 2.0 which were named MOFOF-0.5, MOFOF-1.0, MOFOF-1.5 and MOFOF-2.0, respectively. MOFOF holds the potential to revolutionize gas sensing technologies, particularly in the detection of acidic vapors. The synergistic interaction between the porous framework of MOFs and the electron-rich surface of fullerenes offers enhanced adsorption capacities and rapid response times, contributing to superior sensor performance.

EXPERIMENTAL SECTION

Materials. Pristine fullerene C_{60} (pC_{60}: 99.9%) was procured from BBS Chemicals, USA. Methanol (99.7%), triethylamine (TEA), mesitylene (99.8%), nitric acid (HNO_3:65%), sulfuric acid (H_2SO_4: 98%) were obtained from Wako Chemical Corporation, Tokyo, Japan. Cobalt nitrate

hexahydrate ($Co(NO_3)_2 \cdot 6H_2O$: 99%), and methylimidazole (Mim: 99.8%) were obtained from Tokyo Chemical Industry Co., Ltd., Japan.

Synthesis of FNT. Self-assembled FNT crystals were prepared following the commonly used LLIP method using mesitylene as the 'good' solvent and methanol as the 'bad' solvent. The assembly of fullerene into FNT generally driven by the molecular interactions and self-organization tendencies of the fullerene molecules where the inherent curvature of the fullerene structure along with solvent composition, treatment conditions, and temperature influence the assembly process to form the tubular structures. Solutions of pC_{60} in mesitylene (1.0 mg/mL) were prepared by dissolving the pC_{60} powder applying sonication for 1 h. Undissolved C_{60} was removed by filtration. Methanol (90 mL) was rapidly added into a 150 mL glass vial containing freshly prepared pC_{60} solution in mesitylene (30 mL) and the resulting mixture shaken vigorously by hand for about 5 s, then incubated at 25 °C for 2 h without external mechanical disturbances. The precipitate was separated by centrifugation followed by washing with methanol three times then dried at 80 °C under reduced pressure for 6 h.

Surface modification of FNT. For the surface modification of the FNT, we aimed to ensure that the functionalization process was efficient and did not compromise the structural integrity of the FNTs. We precisely controlled the ratio of oxidizing agents (H_2SO_4/HNO_3), sonication/reaction time, and temperature to prevent potential over-oxidation or structural degradation during the functionalization process. The modification/oxidation of FNT was carried out by simple sonication of the as-synthesized FNT in a mixture of concentrated HNO_3 and H_2SO_4 (1/1 v/v ratio). Typically, FNT (100 mg) was added to concentrated HNO_3/H_2SO_4 (10 mL). The mixture was sonicated for 20 min, separated by centrifugation, washed with water (until washings reach pH ~7), and dried

under reduced pressure at 80 °C for 12 h. The dried acid treated or oxidized FNT (FNT_{ox}) was used to synthesize the MOFOF composites.

Synthesis of MOFOFs. In the synthesis of the MOFOF composites, specific conditions were carefully selected to optimize the quality and functionality of the resulting materials. The method for MOFOF synthesis involves in-situ growth of ZIF-67 onto FNT_{ox} at room temperature under ultrasonication. The synthesis temperature of 25 °C (or room temperature) and non-continuous sonication and hand shaking (~10 sec) at 1 min intervals was selected to facilitate the controlled growth of the ZIF-67 crystals on the FNT_{ox} surface without causing degradation of the fullerene structure. Separate $Co(NO_3)_2{\cdot}6H_2O$ (2 mM; 10 mL) and ligand-modulator (Mim + TEA; 16 mM each; 10 mL) solutions were prepared in water. First, the Co^{2+} solution was added into a dispersion of FNT_{ox} (100 mg/mL) in water. The slurry was held under sonication for 5 min with shaking by hand (~10 sec) at 1 min intervals. Mim + TEA solution was then added rapidly, and the same sonication/shaking regime continued for an additional 15 min. The resulting purple-brown solid was collected by centrifugation then washed with water, methanol (three times), and dried at 80 °C for 12 h under reduced pressure. The composition (MOF : FNT_{ox}: or Co^{2+} : C_{60}) of the MOFOF composites was varied by varying the quantity of FNT_{ox} used. MOFOF composites with varying Co^{2+}/C_{60} ratios (e.g., 0.5, 1.0, 1.5, and 2.0) are respectively referred to in this work as MOFOF-0.5, MOFOF-1.0, MOFOF-1.5 and MOFOF-2.0.

Materials Characterization. MOFOF composites were characterized using scanning electron microscopy (SEM, operated at 10 kV, Hitachi S-4800, Tokyo, Japan), scanning transmission electron microscopy (STEM, operated at 30 kV, Hitachi S-4800, Tokyo, Japan), powder X-ray diffraction (PXRD, operated at 40 kV, Cu-Kα radiation (λ = 0.1541 nm) RINT2000 diffractometer, Rigaku, Tokyo, Japan), Fourier transform infrared (FT-IR) spectroscopy (ATR-FTIR, Nexus 670,

Tokyo, Japan), Raman scattering (NRS-3100 Raman spectrophotometer, JASCO, Tokyo, Japan), and X-ray photoelectron spectroscopy (XPS; Thermo Electron Co. Karlsruhe, Germany, monochromatic Al-Kα radiation of photon energy 15 keV). Nitrogen sorption isotherms were recorded at 77 K (Quantachrome Autosorb-1, Boynton Beach, Florida, USA). Samples for electron microscopy were prepared by dropping suspensions of the samples in isopropyl alcohol onto carbon-coated copper grids followed by drying under reduced pressure at 70 °C.

Vapor Sensing using Quartz Crystal Microbalance (QCM). The QCM technique was employed to investigate the vapor sensing properties of the materials. The frequency shift was monitored using a QCM equipped with a Au-resonator coated with the tested materials during exposure to organic vapors. A QCM resonance frequency of 9 MHz (AT-cut) was used. The frequency stability of the QCM electrode was ±2 Hz in air during a 10 min period. The QCM sensor electrode was prepared by drop-casting of a freshly prepared slurry (2 μL) of the test material in IPA (1 mg/1 mL; sonicated for 30 s prior to drop-casting). The resulting modified electrodes were dried at 70 °C for 5 h under reduced pressure. The Au electrode was then connected to the QCM instrument and exposed to different volatile organic solvents (10 mL) in an open container at room temperature placed inside the QCM chamber. The QCM chamber was sealed prior to measurement to maintain a saturated vapor atmosphere throughout the QCM frequency monitoring experiment. The chamber was opened when the frequency shift reached equilibrium for the desorption of the vapors.

RESULTS

Synthesis and characterization of MOFOF composites. Figure 1 shows scanning electron micrographs (SEM) of FNT, FNT_{ox}, and MOFOFs with different compositions. MOFOF samples

were obtained by the in-situ growth of ZIF-67 (a typical MOF) onto the surface-modified FNT at room temperature under ultrasonication. Morphological stability of the FNT (**Figures 1a,b**) under strong acidic conditions (HNO_3/H_2SO_4 (1:1 v/v)) is assumed based on the intact morphology of the FNT_{ox} (**Figures 1c,d**).

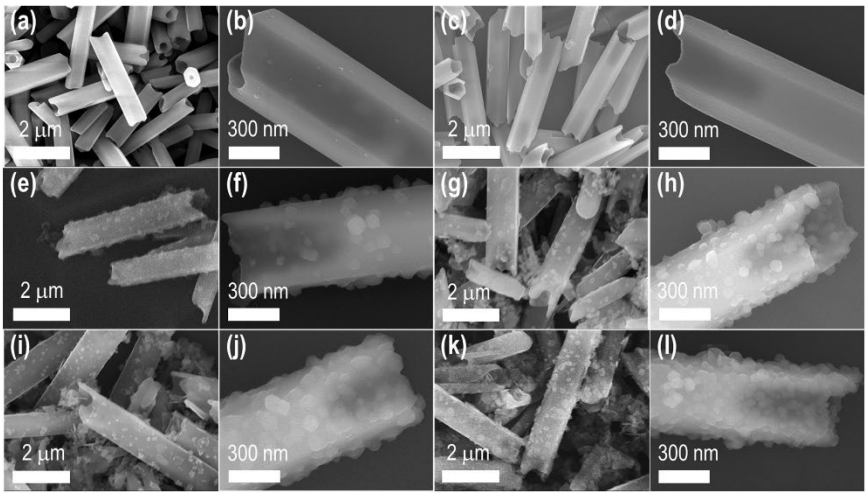

Figure 1. Scanning Electron Microscope (SEM) images depicting the surface morphology of various samples: (a, b) FNT (as synthesized); (c, d) FNT_{ox} (acid treated); (e, f) MOFOF-0.5 (Co^{2+}/C_{60} ratios = 0.5); (g, h) MOFOF-1.0 (Co^{2+}/C_{60} ratios = 1.0); (i, j) MOFOF-1.5 (Co^{2+}/C_{60} ratios = 1.5); and (k, l) MOFOF-2.0 (Co^{2+}/C_{60} ratios = 2.0).

The FNT morphology was maintained with only minor decomposition even following the growth of ZIF-67 crystals onto the surface of the FNT_{ox}. SEM images (**Figures 1e-1l**) of the newly prepared MOFOF composites indicate that ZIF-67 particles grow only at the surfaces of FNT_{ox} with no non-attached particles visible, indicating robust attachment and homogeneous distribution. The uniform distribution of ZIF-67 particles on the FNT_{ox} surfaces and at their interiors is significant for the composite's functional properties, as it ensures maximum surface area and accessibility for various (e.g., catalytic or adsorptive) interactions. Predictably, the quantity of ZIF-

67 particles varies according to the increasing ratio of ZIF-67 precursors. ZIF-67 particles at the exterior of FNT_{ox}, especially for MOFOF-2.0, indicate that there is an optimum Co^{2+}/C_{60} ratio (i.e., Co^{2+}/C_{60}: 1/1) for successful in-situ incorporation of ZIF-67 on the FNT_{ox} in the MOFOF composites.

STEM images of FNT (**Figure 2a**), FNT_{ox} (**Figure 2b**), ZIF-67 (**Figure 2c**), and MOFOF-1.0 (selected as a representative MOFOF; **Figure 2d**) that clearly shows the intact tube morphology and smooth surface after acid treatment, and in-situ decoration by ZIF-67. TEM and HR-TEM images reveal the uniform distribution of ZIF-67 particles (**Figures 2e,f**) on the FNT_{ox} as well as ZIF-67 particles contained at the cavity interiors. This uniform distribution and stable attachment of ZIF-67 particles are crucial for the functional properties of the composites, as it facilitates enhanced interactions with target molecules, leading to high efficiency in applications, especially in hazardous gas sensing.

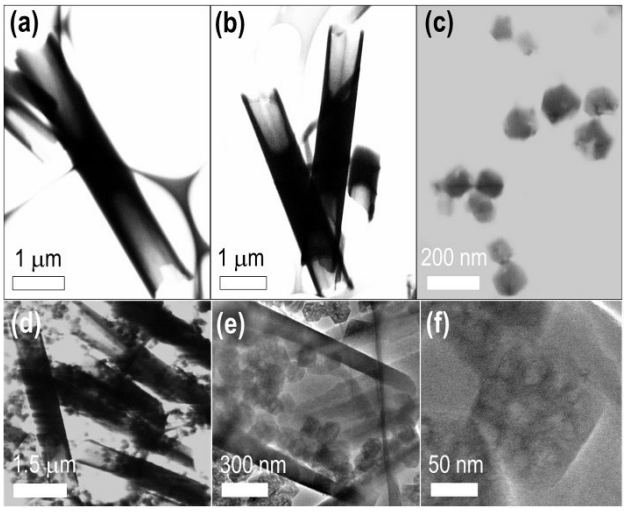

Figure 2. Scanning Transmission Electron Microscopy (STEM) images of (a) FNT, (b) FNT_{ox}, (c) pZIF-67 and (d) MOFOF-1.0. Transmission Electron Microscopy (TEM) (e) and (TEM) and High-Resolution TEM (HR-TEM) (f) image of MOFOF-1.0.

Figure 3a shows the PXRD patterns of the representative MOFOF (MOFOF-1.0), ZIF-67, FNT, and FNT_{ox}. There is no variation in the bulk crystal phase structure of FNT and FNT_{ox} even after acid treatment. Additional peaks appearing in the PXRD pattern of the MOFOF-1.0 are assigned as being due to ZIF-67 (assignment is highlighted with dotted lines in the XRD patterns; **Figure 3a**).

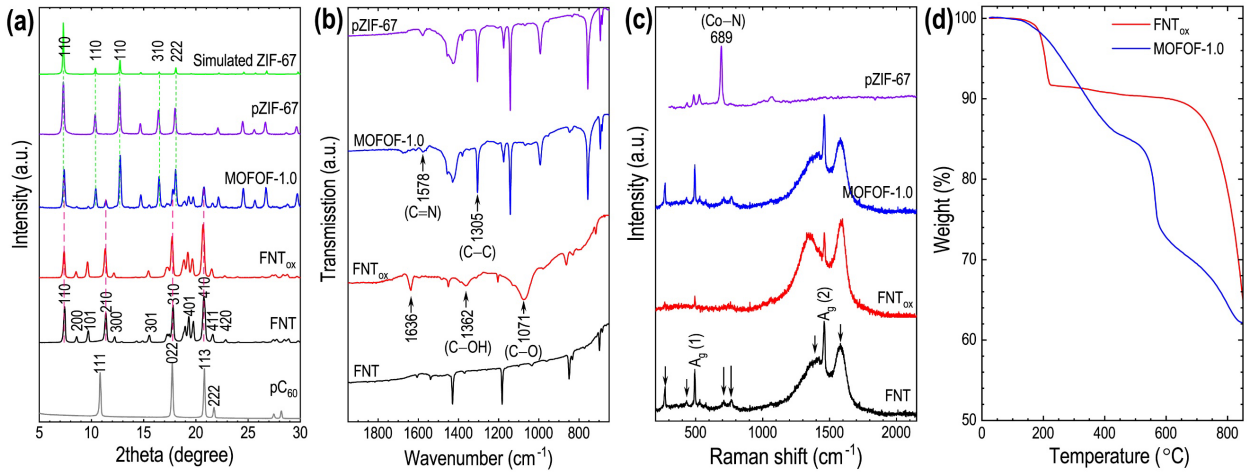

Figure 3. Physical characterization of the materials FNT, FNT_{ox}, MOFOF-1.0 and pZIF-67. (a) Powder XRD patterns, (b) FTIR spectra, (c) Raman spectra, and (d) thermogravimetric analyses (FNT_{ox} and MOFOF-1.0 only).

PXRD peaks corresponding to ZIF-67 in MOFOF-1.0 are further assigned by comparison with the simulated XRD pattern of ZIF-67. **Figure 3b** shows FTIR spectra of MOFOF-1.0, ZIF-67, FNT, and FNT_{ox}. The spectrum of FNT_{ox} has obvious stretching bands at 1070, 1362, and 1636 cm^{-1} originating from C-O (str.), and C-OH (str.), and C=O (str.), respectively[48] due to oxidation or oxy-functionalization at the surfaces of FNT. The FTIR spectrum of the MOFOF-1.0 sample contains additional peaks at 1578 and 1305 cm^{-1} due to C=N (str.) and C-C (str.), respectively, of

the imidazole ring of ZIF-67.[49] **Figure 3c** shows the Raman spectrum of MOFOF-1.0, ZIF-67, FNT, and FNT-ox. Except for a slight broadening of peaks, there are no obvious spectral changes caused by converting FNT to FNT_{ox}. The spectrum of MOFOF-1.0 contains a peak at ~689 cm^{-1} that corresponds to the Co-N bond of ZIF-67 further confirming that MOFOF-1.0 is comprised essentially of MOF and FNT_{ox}. Thermogravimetric analyses of MOFOF-1.0 and FNT_{ox} (**Figure 3d**) reveal that FNT_{ox} undergoes two weight losses at 190 °C (probably desorption of solvent) and 700 °C (decomposition). MOFOF-1.0 undergoes similar weight losses for solvent and fullerene decomposition but with an additional loss due to ZIF-67 decomposition, which occurs at a somewhat higher temperature (550 °C) than pristine ZIF-67 (~425 °C)[50] perhaps due to stabilizing effects of additional ligating groups on FNT_{ox}.

Figure 4 shows X-ray photoelectron spectroscopy (XPS) analysis of FNT_{ox} and MOFOF-1.0. The XPS survey spectra (**Figure 4a**) indicate that both are composed of carbon with partial surface oxidation but MOFOF-1.0 has additional peaks corresponding to cobalt- and nitrogen-containing species originating from ZIF-67.

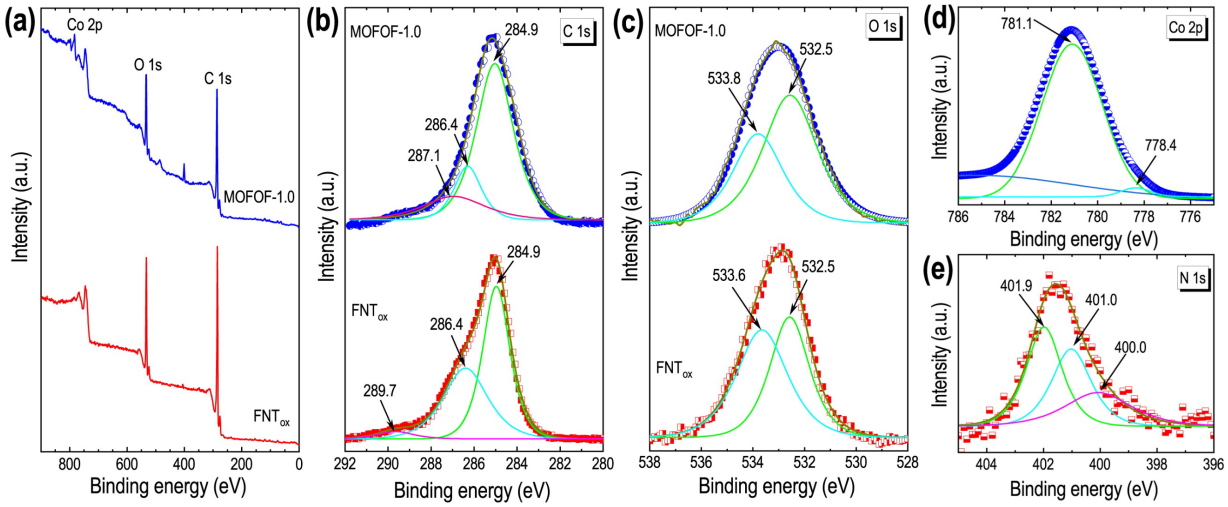

Figure 4. XPS analyses of FNT_{ox} and MOFOF-1.0. (a) XPS survey spectra of FNT-ox and MOFOF-1.0, (b) C 1s core level XPS spectra with the deconvoluted peaks for FNT_{ox}, and

MOFOF-1.0, (c) corresponding O 1s spectra with the deconvoluted peaks, (d) Co 2p spectrum with peak fittings for MOFOF-1.0, and (e) the corresponding N 1s spectrum with peak fittings.

Elemental composition of MOFOF-1.0 were calculated from XPS spectra at 78.3 (carbon), 14.8 (oxygen), 1.0 (nitrogen), and 5.9 (cobalt) atom%. FNT_{ox} contains 83.8 % carbon and 16.2 % oxygen with high oxygen contents in the tested materials originating largely from surface oxidation of the FNT by the strong acid mixture. The deconvoluted C 1s spectrum of the FNT_{ox} contains peaks at 284.9, 286.4, and 289.7 eV due to C=C (sp^2), C-C/C-O (sp^3), and CO_3^{2-} bonding states of carbon with a slight shift from the oxidized pC_{60} (**Figure 4b;** bottom).[48] The O 1s spectrum of FNT_{ox} was deconvoluted as two peaks centered at 532.5 and 533.6 eV assigned to C–OH, and C–O–C bonding states of the oxidized surface also with a slight shift relative to pC_{60} (**Figure 4c;** bottom).[36] The C 1s spectrum of MOFOF-1.0 was deconvoluted as three peaks centered at 285.0, 286.2, and 287.0 eV corresponding to C=C (sp^2), C-C/C-O (sp^3), and C-N bonding states, respectively (**Figure 4b;** bottom). Peaks in the O 1s spectrum at 532.5 eV and 533.8 eV are assigned to C-OH and C-O-C bonding states (**Figure 4c;** top). For Co_{2p}, there is mainly a $Co\text{-}N_4$ bonding state at 781.1 eV accompanied by a satellite peak at 785.4 eV and a low intense peak at the binding energy of 778.4 eV corresponding to $Co\text{-}N_x$ ($x < 4$) (**Figure 4d**).[51] Co-N, C-N and C=N bonds appear in the N 1s spectrum of the MOFOF-1.0 respectively at 400.0 eV, 401.0 eV, and 401.9 eV (**Figure 4e**).

Figure 5a shows the nitrogen adsorption-desorption isotherms of FNT_{ox} and MOFOFs. The nitrogen adsorption-desorption isotherms were recorded at liquid nitrogen temperature (77 K) following sample annealing for 24 h at 120 ºC. Isotherms obtained for MOFOFs are all Type I and FNT_{ox} exhibits Type IV behavior, i.e., MOFOFs are microporous and specific surface area

increases with increasing ZIF-67 content. FNT_{ox} is essentially non-porous. Pore size distribution analysis results obtained by DFT (**Figure 5b**) and BJH (**Figure 5c**) methods are summarized in Table 1.

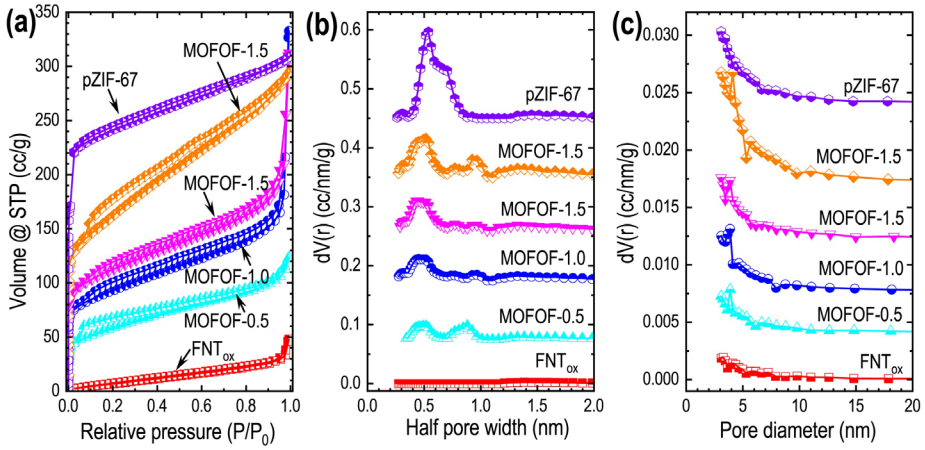

Figure 5. Textural properties of FNT_{ox}, MOFOFs, and pZIF-67 and their components. (a) Nitrogen adsorption-desorption isotherms, pore size distributions curves using (b) the DFT method and (c) the BJH method.

Table 1. Surface area and porosity properties of FNT_{ox}, MOFOFs and pZIF-67.

Sample	S_{BET} (m^2/g)	S_{micro} (m^2/g)	V_{micro} (cm^3/g)	V_p (cm^3/g)	D_p (nm)	W_p (nm)
FNT_{ox}	36.9	18.0	0.050	0.118	1.63	1.38
MOFOF-0.5	199.3	44.5	0.094	0.19	1.94	1.94
MOFOF-1.0	306.6	279.6	0.281	0.658	1.94	0.45
MOFOF-1.5	405.3	331.3	0.321	0.638	1.55	0.45

MOFOF-2.0	543.9	469.4	0.408	0.611	1.55	0.51
pZIF-67	744.7	614.9	0.423	0.535	1.54	0.54

S_{BET} = BET surface area, S_{micro} = micropore surface area, V_{micro} = micropore volume, V_p = total pore volume, D_p = average pore diameter obtained from the BJH analysis, and W_p = average half pore width obtained from the DFT model.

Sensing of organic vapors by Quartz Crystal Microbalance. Figure 6 presents the vapor sensing properties of the MOFOF composites, ZIF-67, and FNT samples obtained using the QCM technique. **Figure 6a** shows the time-dependent frequency shifts (Δf) to the QCM electrodes modified with MOFOF composites, ZIF-67, and FNT samples upon exposure to formic acid (FA) vapor. Generally, rapid frequency shifts are observed upon exposure to FA with a return almost to the initial frequency state when FA vapor is removed from the QCM sensing chamber. Interestingly, for MOFOFs the frequency shift curve does not return to the initial frequency state following cessation of acid vapor exposure (**Figure 6a**), although the frequency curves of sensors prepared from pristine ZIF-67 and FNT materials return rapidly to their starting states after exposure to air. **Figure 6d** shows the sensing properties of the QCM sensor modified with MOFOF-1.0 for a wide range of VOCs where sensitivity/selectivity follows the order formic acid > acetic acid > toluene > benzene > cyclohexane > hexane > pyridine > acetone > aniline.

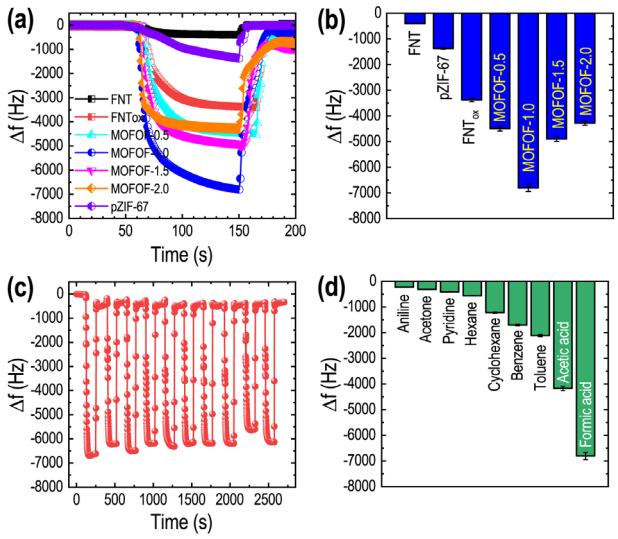

Figure 6. Vapor sensing performance of MOFOFs. (a) QCM frequency shifts (Δf) upon exposure of QCM electrodes modified with FNT, FNT_{ox}, ZIF-67, MOFOF-0.5, MOFOF-1.0, MOFOF-1.5 and MOFOF-2.0 to formic acid vapor. (b) Relative sensing performance of formic acid vapor by the different materials. (c) Reproducibility test upon alternating exposure and removal of formic acid vapor. (d) Relative sensing performance for various organic volatile vapors over the MOFOF-1.0.

DISCUSSION

Preparation and Characterization. MOFOF composites with different compositions were obtained by a two-step in-situ method involving the growth of ZIF-67 crystals on surface-modified FNT at room temperature under ultrasonication for ~15 min. The successful fabrication of the MOFOF composites with varying Co^{2+}/C_{60} ratios (e.g. 0.5, 1.0, 1.5, and 2.0) was confirmed using various characterization techniques. ZIF-67-decorated FNTs are 4 – 5 μm long with diameters in the range 600 – 700 nm with open voids (~500 nm) at their interiors suitable to accommodate polyhedral ZIF-67 crystals in the 50 – 100 nm range. The precise distribution and interconnection

of ZIF-67 particles at the interior/exterior surfaces of FNT can be controlled by controlling the precursor ratio, and the novel MOF-on-fullerene (MOFOF) composite can be rapidly obtained in high yield under ambient reaction conditions. The higher Co^{2+}/C_{60} ratio leads to the formation of unexpected out surface growth of ZIF-67 particles (e.g., MOFOF-2.0) due to the rapid nucleation/crystallization of ZIF-67 crystals at higher precursor concentration. This is the first example of the direct growth of MOF particles onto a fullerene nanostructure. MOF (here ZIF-67) crystals nucleate at the oxidized surfaces of FNT promoting the on-surface growth of ZIF-67 crystals and maintaining connectivity of the two components.

The interaction between the fullerene nanotubes (FNT_{ox}) and the metal-organic framework (MOF) is primarily assumed to be non-covalent. Since the Co^{2+} solution was added first, followed by the ligand solution, the FNT_{ox} enriched with electronegative charges initially interacted with the Co^{2+} ions. Once the ligand was added, it coordinated with the metal ions to form ZIF-67. Therefore, the electrostatic interaction between the positively charged Co^{2+} and the negatively charged FNT_{ox}, as well as the π-π interactions with the imidazole linkers of the MOF, facilitated a strong attachment of the MOF on the FNT surface.

Morphological analyses reveal the successful incorporation and uniform distribution of ZIF-67 crystals (**Figure 1 and Figure 2**) throughout the MOFOFs, and PXRD and Raman analyses demonstrate the successful combination of ZIF-67 and FNT_{ox} as a well-integrated nanostructure. The composite also has improved thermal stability over pristine ZIF-67. XPS analysis of the MOFOF indicates C-N, C=N, and Co-N_4 bonding states that further confirm the integration of ZIF-67 crystals into the FNT nanostructure. The low intensity XPS peak at 778.4 eV corresponds to Co-N_x ($x < 4$) indicating trace defect sites of uncoordinated Co(II) and 2-methyl-imidazole (basic N-sites) within the ZIF-67 crystals.[51] Analysis of the textural properties of MOFOFs

(**Figure 5** and **Table 1**) indicate a bimodal pore architecture for the composites. Defect sites and designer pore architectures are essential features to establish interactions with guest molecules in sensing operations since they promote the close approach and binding of analyte species, in this case, volatile organic compounds.

Sensing of Organic Vapors. QCM results suggest strong irreversible interactions between the acidic and basic sites (uncoordinated N-sites) of imidazole ligands contained in ZIF-67 of the MOFOF nanocomposites, which is beneficial for the adsorption of reactive species such as volatile organic acids molecules through acid-base interactions. Of the MOFOFs tested, MOFOF-1.0 exhibits superior sensitivity for acid vapors and can be regarded as an optimized MOFOF nanocomposite for efficient acid vapor sensing. **Figure 6c** shows a reproducibility test during alternating exposure and removal of FA. It suggests excellent efficiency of the MOFOF-1.0 modified QCM substrate for FA sensing with excellent repeatability. The high sensitivity and selectivity of MOFOF-1.0 for acid vapor over other aromatic or neutral VOCs strongly suggests the operation of a specific chemical reaction such as acid-base interactions[52,53] facilitated by the micro- and mesopores channels, interfacial facets, and defect sites. Of the materials studied here, MOFOF-1.0 is the most sensitive composite for FA sensing using the QCM technique.

CONCLUSION

A new porous MOFOF composite with uniform distribution of ZIF-67, a typical MOF, grown on self-assembled FNT_{ox}, was synthesized following a two-step in-situ method. By varying the ratio of FNT and MOF precursors, in particular the Co^{2+}/C_{60} ratio, the distribution and interconnectedness of the MOFOF components can be controlled by this simple room temperature synthesis procedure using a standard ultrasound bath. The resulting MOFOFs possess large

specific surface areas based on of micro- and mesopore channels, contain defect sites for binding of guest molecules, and show excellent sensitivity for acid vapor sensing when applied in as QCM sensing layers. These newly developed MOFOF nanocomposites have attractive structural, textural, and chemical features and are anticipated to be useful in a wide range of potential applications beyond the sensing application discussed here. Moreover, the future direction of this discovery could focus on optimizing the synthesis process (e.g., from in-situ to layer-by-layer) to further enhance the structural integrity and functional properties of MOFOF composites. Additionally, exploring integrating other types of MOFs with different fullerene-based nanostructures may yield composites with tailored functionalities for diverse applications such as catalysis, gas storage, and environmental remediation.

AUTHOR INFORMATION

Corresponding Authors

Lok Kumar Shrestha (Email: SHRESTHA.Lokkumar@nims.go.jp)

Katsuhiko Ariga (Email: ARIGA.Katsuhiko@nims.go.jp)

Authors

Biswa Nath Bhadra − *Research Center for Materials Nanoarchitectonics (WPI-MANA), National Institute for Materials Science (NIMS), Tsukuba, Ibaraki 305-0044, Japan*; https://orcid.org/0000-0001-7268-2563

Lok Kumar Shrestha − *Research Center for Materials Nanoarchitectonics (WPI-MANA), National Institute for Materials Science (NIMS), Tsukuba, Ibaraki 305-0044, Japan and Department of Materials Science, Institute of Pure and Applied Sciences, University of Tsukuba, Tsukuba 305-8573, Ibaraki, Japan*; https://orcid.org/0000-0003-2680-6291

Renzhi Ma− *Research Center for Materials Nanoarchitectonics (WPI-MANA), National Institute for Materials Science (NIMS), Tsukuba, Ibaraki 305-0044, Japan;*

Jonathan P. Hill− *Research Center for Materials Nanoarchitectonics (WPI-MANA), National Institute for Materials Science (NIMS), Tsukuba, Ibaraki 305-0044, Japan; https://orcid.org/0000-0002-4229-5842*

Yusuke Yamauchi – *Department of Materials Process Engineering, Graduate School of Engineering, Nagoya University, Nagoya 464−8603, Japan, Department of Chemical and Biomolecular Engineering, Yonsei University, 50 Yonsei-ro, Seodaemun-gu, Seoul 03722, South Korea and Australian Institute for Bioengineering and Nanotechnology (AIBN) and School of Chemical Engineering, The University of Queensland, Brisbane, Queensland 4072, Australia;*

Katsuhiko Ariga − *Research Center for Materials Nanoarchitectonics (WPI-MANA), National Institute for Materials Science (NIMS), Tsukuba, Ibaraki 305-0044, Japan and Department of Advanced Materials Science, Graduate School of Frontier Sciences, The University of Tokyo, Chiba 277-8561, Japan*; https://orcid.org/0000-0002-2445-2955

Author Contributions

L.K.S. and K.A. contributed to conceptualization, B.N.B., L.K.S., R.M., J.P.H., Y.Y. and K.A. contributed to methodology, B.N.B, R.M., and L.K.S. contributed to investigation, B.N.B., L.K.S., J.P.H., Y.Y., and R.M., contributed to data curation, B.N.B, and L.K.S. contributed to writing original draft preparation, L.K.S., J.P.H., Y.Y., and K.A. contributed to review and editing, L.K.S.,

and K.A. contributed to supervision and project administration, Y.Y. and K.A. contributed to funding acquisition. All authors have read and agreed to the published version of the manuscript.

Notes

The authors declare no competing financial interest.

ACKNOWLEDGMENT

This study was partially supported by Japan Society for the Promotion of Science KAKENHI Grant Numbers, JP20H00392 and JP23H05459. The authors are grateful to JST-ERATO Yamauchi Materials Space-Tectonics Project (JPMJER2003) and the Queensland Node of the Australian National Fabrication Facility (ANFF-Q).

REFERENCES

1. Zhou, H. C. J.; Kitagawa, S. Metal–Organic Frameworks (MOFs). *Chem. Soc. Rev.* **2014**, *43*, 5415–5418. DOI:10.1039/C4CS90059F
2. Furukawa, H.; Cordova, K. E.; O'Keeffe, M.; Yaghi, O. M. The Chemistry and Applications of Metal-Organic Frameworks. *Science* **2013**, *341* (6149), 1230444. DOI: 10.1126/science.1230444
3. Bhadra, B. N.; Ahmed, I.; Lee, H. J.; Jhung, S. H. Metal-Organic Frameworks Bearing Free Carboxylic Acids: Preparation, Modification, and Applications. *Coord. Chem. Rev.* **2022**, *450* (January), 214237. DOI: 10.1016/J.CCR.2021.214237
4. Shi, L.; Kirlikovali, K. O.; Chen, Z.; Farha, O. K. Metal-Organic Frameworks for Water Vapor Adsorption. *Chem.* **2024**, *10* (2) 484–503. DOI: 10.1016/j.chempr.2023.09.005
5. Li, H.; Wang, K.; Sun, Y.; Lollar, C. T.; Li, J.; Zhou, H. C. Recent Advances in Gas Storage

and Separation Using Metal–Organic Frameworks. *Mater. Today* **2018**, *21* (2) 108–121. DOI: 10.1016/j.mattod.2017.07.0066

6. Zhao, X. ; Wang, Y.; Li, D. S.; Bu, X.; Feng, P. Metal–Organic Frameworks for Separation, Adv. Mater. **2018**, *30*, 1705189. DOI: 10.1002/adma.201705189
7. Shen, Y.; Tissot, A.; Serre, C. Recent Progress on MOF-based Optical Sensors for VOC Sensing. *Chem. Sci.* **2022**, *13* (47), 13978–14007. DOI: 10.1039/d2sc04314a
8. Zhu, Q. L.; Xu, Q. Metal–Organic Framework Composites. *Chem. Soc. Rev.* **2014**, *43* (16) 5468–5512. DOI: 10.1039/C3CS60472A
9. Xue, Y.; Zheng, S.; Xue, H.; Pang, H. Metal–Organic Framework Composites and Their Electrochemical Applications. *J. Mater. Chem. A.* **2019**, *7* (13) 7301–7327. DOI: 10.1039/C8TA12178H
10. Chen, L.; Xu, Q. Metal-Organic Framework Composites for Catalysis. Matter. **2019**, *1* (1) 57–89. DOI: 10.1016/j.matt.2019.05.018
11. Huang, P.; Wu, W.; Li, M.; Li, Z.; Pan, L.; Ahamad, T. ; Alshehri, S. M.; Bando, Y.; Yamauchi, Y.; Xu, X. Metal-Organic Framework-Based Nanoarchitectonics: A Promising Material Platform for Electrochemical Detection of Organophosphorus Pesticides. *Coord. Chem. Rev.* **2024**, *501* (February) 215534. DOI: 10.1016/j.ccr.2023.215534
12. Tatrari, G.; An, R.; Shah, F. U. Designed Metal-Organic Framework Composites for Metal-Ion Batteries and Metal-Ion Capacitors. *Coord. Chem. Rev.* **2024**, *512* (August) 215876. DOI: 10.1016/j.ccr.2024.215876
13. Kalaj, M.; Bentz, K. C.; Ayala, S. J.; Palomba, J. M.; Barcus, K. S.; Katayama, Y.; Cohen, S. M. MOF-polymer Hybrid Materials: From Simple Composites to Tailored Architectures. *Chem. Rev.* **2020**, *120* (16) 8267–8302. DOI: 10.1021/acs.chemrev.9b00575

14. Wang, D.; Li, T. Toward MOF@polymer Core–Shell Particles: Design Principles and Potential Applications, *Acc. Chem. Res.* **2023**, *56* (4) 462–474. DOI: 10.1021/acs.accounts.2c00695

15. Xiang, W.; Zhang, Y.; Lin, H.; Liu, C. Nanoparticle/Metal–Organic Framework Composites for Catalytic Applications: Current Status and Perspective, *Molecules* **2017**, 22 (12), 2103. DOI: 10.3390/molecules22122103

16. Liu, K. G.; Bigdeli, F.; Panjehpour, A.; Jhung, S. H.; Al Lawati H. A. J.; Morsali, A. Potential Applications of MOF Composites as Selective Membranes for Separation of Gases. *Coord. Chem. Rev.* **2023**, *496* (December) 215413. DOI: 10.1016/j.ccr.2023.215413.

17. Liu, X. W.; Sun, T. J.; Hu, J. L.; Wang, S. D. Composites of Metal–Organic Frameworks and Carbon-Based Materials: Preparations, Functionalities and Applications. *J. Mater. Chem. A.* **2016**, *4* (10) 3584–3616. DOI: 10.1039/C5TA09924B

18. Parsapour, F.; Moradi, M.; Safarifard, V.; Sojdeh, S. Polymer/MOF Composites for Metal-Ion Batteries: A Mini Review. *J. Energy Storage.* **2024**, *82* (March) 110487. DOI: 10.1016/j.est.2024.110487

19. Chen, J. Q.; Sharifzadeh, Z.; Bigdeli, F.; Gholizadeh, S.; Li, Z.; Hu, M. L.; Morsali, A. MOF Composites as High Potential Materials for Hazardous Organic Contaminants Removal in Aqueous Environments. *J. Environ. Chem. Eng.* **2023**, *11* (2) 109469. DOI: 10.1016/j.jece.2023.109469

20. Ji, Y.; You, Y.; Xu, G.; Yang, X.; Liu, Y. Engineering Metal Organic Framework (MOF)@Mxene Based Electrodes for Hybrid Supercapacitors – A Review. *Chem. Eng. J.* **2024**, *483* (March) 149365. DOI: 10.1016/j.cej.2024.149365

21. Yusuf, M.; Kumar, R.; Khan, M. A.; Ahmed, M. J.; Otero, M.; Prabhu, S. M.; Son, M.;

Hwang, J. H.; Lee, W. H.; Jeon, B. H. Metal-Organic Framework-Based Composites for Biogas and Natural Gas Uptake: An Overview of Adsorption and Storage Mechanisms of Gaseous Fuels. *Chem. Eng. J.* **2023**, *478* (December) 147302. DOI: 10.1016/j.cej.2023.147302

22. Tehrani, M. M.; Chehrazi, E. Metal–Organic-Frameworks Based Mixed-Matrix Membranes for CO_2 Separation: An Applicable-Conceptual Approach. *ACS Appl. Mater. Interfaces* **2024**, *16*(26), 32906–32929. DOI: 10.1021/acsami.4c06931
23. Ariga, K. Nanoarchitectonics: The method for Everything in Materials Science. *Bull. Chem. Soc. Jpn.* **2023**, *97* (1) uoad001. DOI: 10.1093/bulcsj/uoad001
24. Ariga, K.; Nishikawa, M.; Mori, T.; Takeya, J.; Shrestha, L. K.; Hill, J. P. Self-Assembly as a Key Player for Materials Nanoarchitectonics. *Sci. Technol. Adv. Mater.* **2019**, 20 (1) 51–95. DOI: 10.1080/14686996.2018.1553108
25. Ariga, K.; Mori, T.; Kitao, T.; Uemura, T. Supramolecular Chiral Nanoarchitectonics. *Adv. Mater.* **2020**, *32* (41) 1905657. DOI: 10.1002/ADMA.201905657
26. Baskar, A. V.; Benzigar, M. R.; Talapaneni, S. N.; Singh, G.; Karakoti, A. S.; Yi, J.; Al-Muhtaseb, A. H.; Ariga, K.; Ajayan, P. M.; Vinu, A. Self-Assembled Fullerene Nanostructures: Synthesis and Applications. *Adv. Funct. Mater.* **2022**, *32* (6) 2106924. DOI: 10.1002/ADFM.202106924
27. Maji, S.; Shrestha, L. K.; Ariga, K. Nanoarchitectonics for Hierarchical Fullerene Nanomaterials. *Nanomater.* **2021**, *11* (8), 2146. DOI: 10.3390/NANO11082146
28. Chen, G.; Sciortino, F.; Takeyasu, K.; Nakamura, J.; Hill, J. P.; Shrestha, L. K.; Ariga, K. Hollow Spherical Fullerene Obtained by Kinetically Controlled Liquid-Liquid Interfacial Precipitation. *Chem. Asian J.* **2022**, *17* (20) e202200756. DOI: 10.1002/asia.202200756

29. Jin, Y.; Curry, R. J.; Sloan, J.; Hatton, R. A.; Chong, L. C.; Blanchard, N.; Stolojan, V.; Kroto, H. W.; Silva, S. R. P. Structural And Optoelectronic Properties of C_{60} Rods Obtained via a Rapid Synthesis Route. *J. Mater. Chem.* **2006**, *16* (37) 3715–3720. DOI: 10.1039/B609074E.

30. Sathish, M.; Miyazawa, K.; Sasaki, T. Nanoporous Fullerene Nanowhiskers. *Chem. Mater.* **2007**, *19* (10) 2398–2400. DOI:10.1021/cm070114a

31. Minato, J.; Miyazawa, K.; Suga, T. Morphology of C_{60} Nanotubes Fabricated by The Liquid–Liquid Interfacial Precipitation Method. *Sci. Technol. Adv. Mater.* **2005**, *6* (3-4) 272–277. DOI: 10.1016/j.stam.2005.02.006

32. Hill, J. P.; Shrestha, R. G.; Song, J.; Ji, Q.; Ariga, K.; Shrestha, L. K. Monitoring the Release of Silver from a Supramolecular Fullerene C_{60}-$AgNO_3$ Nanomaterial. *Bull. Chem. Soc. Jpn.* **2021**, *94* (4) 1347–1354. DOI: 10.1246/bcsj.20210028

33. Park, C.; Yoon, E.; Kawano, M.; Joo, T.; Choi, H. C. Self-Crystallization of C_{70} Cubes and Remarkable Enhancement of Photoluminescence. *Angew. Chemie Int. Ed.* **2010**, *49* (50) 9670–9675. DOI: 10.1002/anie.201005076

34. Osonoe, K.; Kano, R.; Miyazawa, K.; Tachibana, M. Synthesis of C_{70} Two-Dimensional Nanosheets by Liquid–Liquid Interfacial Precipitation Method. *J. Cryst. Growth.* **2014**, *401* (September) 458–461. DOI: 10.1016/j.jcrysgro.2013.12.056

35. Chen, N.; Hu, Y.; Xu, T.; Lu, X. Three-Dimensional "Star of David"-Shaped Fullerene (C60) Microstructures: Controlled Synthesis, Photoluminescence, and Photoelectrochemical Properties. *ACS Appl. Electron. Mater.* **2020**, *2* (7) 2010–2016. DOI: 10.1021/acsaelm.0c00290

36. Chen, G.; Bhadra, B. N.; Sutrisno, L.; Shrestha, L. K.; Ariga, K. Fullerene Rosette: Two-

Dimensional Interactive Nanoarchitectonics and Selective Vapor Sensing. *Int. J. Mol. Sci.* **2022**, *23* (10), 5454. DOI: 10.3390/ijms23105454

37. Neal, E. A.; Nakanishi, T. Alkyl-Fullerene Materials of Tunable Morphology and Function. *Bull. Chem. Soc. Jpn.* **2021**, *94* (6) 1769–1788. DOI:10.1246/bcsj.20210129
38. Bairi, P.; Minami, K.; Hill, J. P.; Nakanishi, W.; Shrestha, L. K.; Liu, C.; Harano, K.; Nakamura, E.; Ariga, K. Supramolecular Differentiation for Construction of Anisotropic Fullerene Nanostructures by Time-Programmed Control of Interfacial Growth. ACS Nano. 2016, 10 (9) 8796–8802. DOI: 10.1021/acsnano.6b04535
39. Ge, L.; Yang, Y.; Wang, L.; Zhou, W.; De Marco, R.; Chen, Z.; Zou, J.; Zhu, Z. High Activity Electrocatalysts from Metal–Organic Framework-Carbon Nanotube Templates for the Oxygen Reduction Reaction. *Carbon* **2015**, *82* (February) 417–424. DOI: 10.1016/j.carbon.2014.10.085
40. Chen, K.; Sun, Z.; Fang, R.; Shi, Y.; Cheng, H. M.; Li, F. Metal–Organic Frameworks (MOFs)-Derived Nitrogen-Doped Porous Carbon Anchored on Graphene with Multifunctional Effects for Lithium–Sulfur Batteries. *Adv. Funct. Mater.* **2018**, *28* (38) 1707592. DOI: 10.1002/adfm.201707592
41. Chronopoulos, D. D.; Saini, H.; Tantis, I.; Zbořil, R.; Jayaramulu, K.; Otyepka, M. Carbon Nanotube Based Metal–Organic Framework Hybrids from Fundamentals Toward Applications. *Small* **2022**, *18* (4) 2104628. DOI: 10.1002/smll.202104628
42. Ohmura, T.; Usuki, A.; Mukae, Y.; Motegi, H.; Kajiya, S.; Yamamoto, M.; Senda, S.; Matsumoto, T.; Tatsumi, K. Supramolecular Porphyrin-Based Metal–Organic Frameworks with Fullerenes: Crystal Structures and Preferential Intercalation of C_{70}. *Chem. Asian J.* **2016**, *11* (5) 700–704. DOI: 10.1002/asia.201501422

43. Li, H.; Hill, M. R.; Huang, R.; Doblin, C.; Lim, S.; Hill, A. J.; Babarao, R.; Falcaro, P. Facile Stabilization of Cyclodextrin Metal–Organic Frameworks under Aqueous Conditions via the Incorporation of C_{60} in Their Matrices. *Chem. Commun.* **2016**, *52* (35) 5973–5976. DOI: 10.1039/C6CC01620K

44. Martinez, V.; Karadeniz, B.; Biliškov, N.; Lončarić, I.; Muratović, S.; Žilić, D. ; Avdoshenko, S. M.; Roslova, M.; Popov, A. A.; Užarević, K. Tunable Fulleretic Sodalite MOFs: Highly Efficient and Controllable Entrapment of C_{60} Fullerene via Mechanochemistry. *Chem. Mater.* **2020**, *32* (24) 10628–10640. DOI: 10.1021/acs.chemmater.0c03796

45. Zhang, H. W.; Li, H. K.; Han, Z. Y.; Yuan, R.; He, H. Incorporating Fullerenes in Nanoscale Metal–Organic Matrixes: An Ultrasensitive Platform for Impedimetric Aptasensing of Tobramycin. *ACS Appl. Mater. Interfaces* **2022**, *14* (5) 7350–7357. DOI: 10.1021/acsami.1c23320

46. Han, J.; Wu, H.; Fan, H.; Ding, L.; Hai, G.; Caro, J.; Wang, H. Tuning the Phase Composition of Metal–Organic Framework Membranes for Helium Separation through Incorporation of Fullerenes. *J. Am. Chem. Soc.* **2023**, *145* (27) 14793–14801. DOI: 10.1021/jacs.3c03362

47. Niu, X.; Liu, Y.; Zhao, R.; Yuan, M.; Zhao, H.; Li, H.; Wang, K. Enhancing Electrochemical Signal for Efficient Chiral Recognition by Encapsulating C_{60} Fullerene into Chiral Lanthanum-Based MOFs Enhancing Electrochemical Signal for Efficient Chiral Recognition by Encapsulating C_{60} Fullerene into Chiral Lanthanum-Based MOFs. *ACS Appl. Mater. Interfaces* **2024**, *16* (14), 17361–17370. DOI: 10.1021/acsami.4c03134

48. Zygouri, P.; Spyrou, K.; Mitsari, E.; Barrio, M.; Macovez, R.; Patila, M.; Stamatis, H.;

Verginadis, I. I.; Velalopoulou, A. P.; Evangelou, A. M. ; Sideratou, Z.; Gournis, D.; Rudolf, P. A Facile Approach to Hydrophilic Oxidized Fullerenes and Their Derivatives as Cytotoxic Agents and Supports aor Nanobiocatalytic Systems. *Sci. Rep.* **2020**, *10* (May) 8244. DOI: 10.1038/s41598-020-65117-7

49. Han, H.; Yuan, X.; Zhang, Z.; Zhang, J. Preparation of a ZIF-67 Derived Thin Film Electrode via Electrophoretic Deposition for Efficient Electrocatalytic Oxidation of Vanillin. *Inorg. Chem.* **2019**, *58* (5) 3196–3202. DOI: 10.1021/acs.inorgchem.8b03281
50. Wu, H.; Qian, X.; Zhu, H.; Ma, S.; Zhu, G.; Long, Y. Controlled Synthesis of Highly Stable Zeolitic Imidazolate Framework-67 Dodecahedra and Their Use Towards The Templated Formation of a Hollow Co_3O_4 Catalyst for CO Oxidation. *RSC Adv.* **2016**, *6* (9) 6915–6920. DOI: 10.1039/C5RA18557B
51. Tao, L.; Lin, C. Y.; Dou, S.; Feng, S.; Chen, D.; Liu, D.; Huo, J.; Xia, Z.; Wang, S. Creating Coordinatively Unsaturated Metal Sites in Metal-Organic-Frameworks as Efficient Electrocatalysts for the Oxygen Evolution Reaction: Insights into the Active Centers. *Nano Energy.* **2017**, *41* (November) 417–425. DOI: 10.1016/j.nanoen.2017.09.055
52. Ahmed, L. R.; Lüder, J.; Chuang, C.-H.; Chuang, C.-H.; EL-Mahdy, A. F. M. Covalent-Organic-Framework-Modified Quartz Crystal Microbalance Sensor for Selective Detection of Hazardous Formic Acid. *ACS Appl. Mater. Interfaces* **2024**, *16*(23) 30408–30420. DOI: 10.1021/acsami.4c04630
53. Song, J.; Murata, T.; Tsai, K.-C.; Jia, X.; Sciortino, F.; Ma, R.; Yamauchi, Y.; Hill, J. P.; Shrestha, L. K.; Ariga, K. Fullerphene Nanosheets: A Bottom-Up 2D Material forSingle-Carbon-Atom-Level Molecular Discrimination. *Adv. Mater. Interfaces* **2022**, *9*, 2102241. DOI: 10.1002/admi.202102241

Table of Contents (TOC) graphic